



Alexandria University
Alexandria Engineering Journal

www.elsevier.com/locate/aej
www.sciencedirect.com



ORIGINAL ARTICLE

Analysis of flow behaviour in a two sided lid driven cavity using lattice boltzmann technique

S. Arun, A. Satheesh *

Energy Division, School of Mechanical and Building Sciences, VIT University, Vellore, Tamil Nadu 632014, India

Received 18 March 2015; revised 9 June 2015; accepted 13 June 2015

KEYWORDS

Lattice Boltzmann Method;
 D2Q9 model;
 SRT-BGK approximation

Abstract The flow characteristics of lid-driven cavity are simulated using the Lattice Boltzmann Method (LBM). For achieving the best numerical stability, this problem is solved using two-dimensional nine directional lattice model (D2Q9). Single Relaxation Time-BGK approximation is used for collision of particles. The effect of various Reynolds numbers (100, 1000, 2000 and 5000) and aspect ratios (1, 2 and 4) in the flow characteristics is studied. In this problem two cases of boundary conditions are considered, in the first case, the top and bottom walls move in the same direction towards right side with uniform velocity ($u = 0.1$) and in the second case, the walls move in opposite direction with same velocity. For validation, velocities and the locations of primary, secondary, ternary vortexes obtained from the simulation are compared with existing literatures and found to be in good agreement. The results show that at higher Reynolds number (Re), there is a formation of secondary and ternary vortexes. The shape and size of the vortexes changes with increase in aspect ratio (K). For lower Re, primary vortexes only were observed. However, at low Re with increase in K , there is a formation of secondary vortexes. The pressure contours are also presented.

© 2015 Faculty of Engineering, Alexandria University. Production and hosting by Elsevier B.V. This is an open access article under the CC BY-NC-ND license (<http://creativecommons.org/licenses/by-nc-nd/4.0/>).

1. Introduction

LBM is one of the engineering methods in computational fluid dynamic field. It is the mesoscopic method and one of the most recent simulation techniques based on molecular theory. It is a bottom-up approach that uses the kinetic model at the microscopic level and the transport equations at the macroscopic

level. LBM with the BGK collision model has achieved great success in simulating many fluid flow problems. However, this model suffers from numerical instability for higher Reynolds numbers. Therefore, multiple relaxation time (MRT) models are considered for complex flow and heat transfer problems as it gives better stability. LBM is also one of the most effective among the pseudo-kinetic algorithms. It was used for simulation of fluid flow in a broad range of engineering applications such as single and multiphase flow [1], flow using nanofluids [2] and solving difficult problems with complex geometries [3]. Many complicated problems such as bubble growth and departure from the superheated wall can also be simulated using LBM [4], free convection heat transfer between a cold square

* Corresponding author. Tel.: +91 9597872825.

E-mail addresses: satheesh.a@vit.ac.in, egsatheesh@gmail.com (A. Satheesh).

Peer review under responsibility of Faculty of Engineering, Alexandria University.

<http://dx.doi.org/10.1016/j.aej.2015.06.005>

1110-0168 © 2015 Faculty of Engineering, Alexandria University. Production and hosting by Elsevier B.V.

This is an open access article under the CC BY-NC-ND license (<http://creativecommons.org/licenses/by-nc-nd/4.0/>).

Nomenclature

c_i discrete lattice velocity in the i^{th} direction
 Ω collision factor
 f_i particle distribution function
 f_i^{eq} equilibrium distribution
 \tilde{f}_i post collision distribution function
 t time (s)
 U velocity of lid (m/s)
 u, v dimensionless velocity components at X and Y direction
 ω_i weighing factor in i^{th} direction

Greek symbols

β number of discrete velocities
 ρ density (kg/m^3)
 τ lattice relaxation time
 Δt lattice time-step

Subscripts

i discrete lattice direction

Superscripts

eq equilibrium

and heated elliptic cylinders in the presence of a magnetic field is also investigated [5], analysis of the melting process with natural convection in an inclined cavity has been performed using the enthalpy-based LBM [6]. Literature shows the calculation procedure in LBM is simpler, and parallel computing is possible [7].

The Lid driven cavity flow has been considered as the benchmark problem for a long time to test or validate the coding or new solution methods in the computational field. For testing, this problem is mostly used, because of the abundant

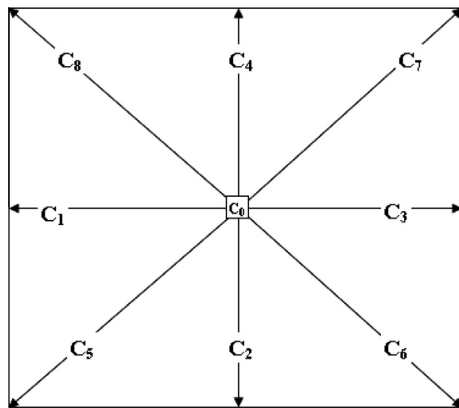


Figure 1 D2Q9 lattice arrangements.

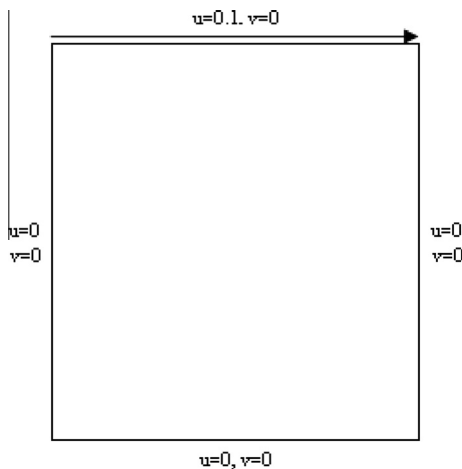


Figure 2 Boundary conditions for code validation.

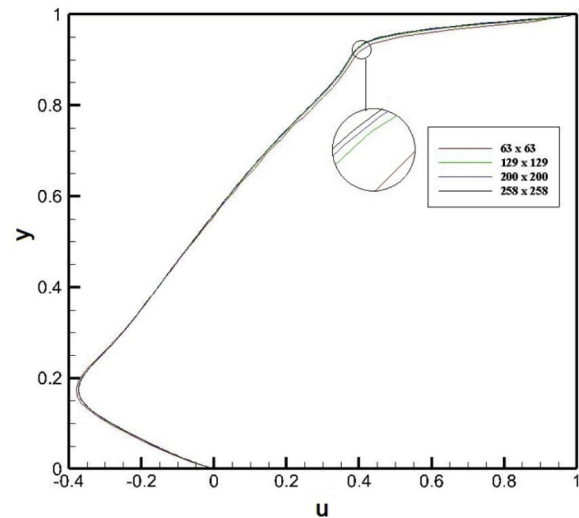
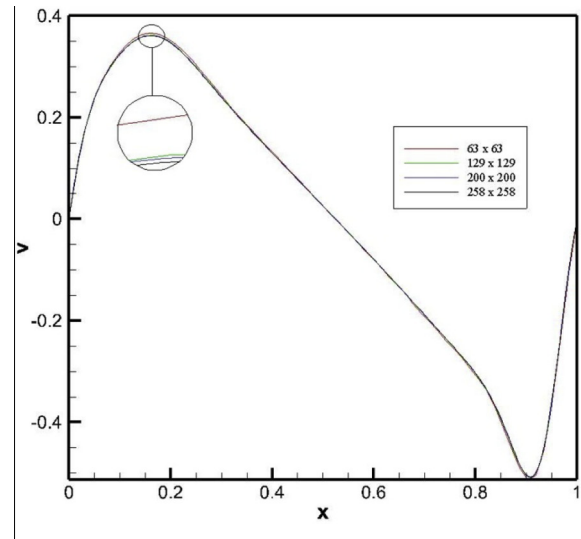


Figure 3 Grid independence test.

Table 1 Comparisons of the locations of the vortices at Reynolds number 1000 for various grid sizes.

Grid size	Primary vortex		Right secondary vortex		Left secondary vortex	
	x	y	x	y	x	y
63 × 63	0.5312	0.5608	0.8672	0.1111	0.0828	0.0766
129 × 129	0.5315	0.5632	0.8664	0.1119	0.0826	0.0767
200 × 200	0.5315	0.5641	0.8663	0.1120	0.0826	0.0767
258 × 258	0.5315	0.5644	0.8663	0.1121	0.0826	0.0767

literatures available to compare the results and the boundary conditions are simple and compatible with most of the numerical approaches. Lid driven cavity flows are important in many industrial processing applications such as short-dwell and flexible blade coaters [8]. Many researchers have studied cavity flow simulation. Hou et al. [9] have studied the cavity flow for various Reynolds numbers using LB-BGK model. Mussa et al. [10] investigated the deep and shallow cavity flow and compared the results with FLUENT software. Taghilou [11] studied the cavity flow for different aspect ratio and various Reynolds numbers. Lin et al. [12] have simulated the cavity flow with MRT model for various aspect ratios, and various Reynolds numbers ranging from 100 to 7500. Yang et al. [13] investigated the flow pattern in lid-driven semi-circular cavity using the MRT model for higher Reynolds numbers ranging from 5000 to 50000, and the results show the stability of the MRT model for a higher Reynolds number as mentioned in the above section. Teamah et al. [28] studied the mixed convection in a rectangular lid driven cavity under the combined buoyancy effects of thermal and mass diffusion. They also studied the double diffusion mixed convection in shallow inclined cavity [31] and mixed convection in two sided lid-driven differentially heat rectangular enclosure [32]. Oueslati [29] in his work studied the double diffusive natural convection and entropy generation in an enclosure of aspect

ratio 4 with partial vertical heating and salting sources. In the deep cavity area with two walls moving in the same and opposite direction conditions, only a few researchers have worked. Hence, in this paper the lid-driven deep cavity flow simulation with various wall motions for different Re ranges from 100 to 5000 and at different K- 1, 2 and 4 are studied by LB-BGK model. The streamline patterns, horizontal velocity, vertical velocity and pressure contours are studied in detail for the parameters mentioned above.

2. Numerical method

A D2Q9 model in LBM is used to solve the lid driven cavity flow problem. The D2Q9 lattice structure is shown in Fig. 1. Since simple geometry is used, BGK collision factor is adopted for this problem. The Boltzmann transport equation is given in Eq. (1) [14].

$$\frac{\partial f}{\partial t} + c \cdot \nabla f = \Omega \quad (1)$$

where f denotes the particle distribution function, t indicates the time, c is the particle velocities and Ω is the Boltzmann collision factor. The Boltzmann collision factor is very complicated to use in the code because of the complicated structure. In order to overcome that various researchers found different collision factors with various relaxation time such as single [15], two [16], and multiple relaxation times [17,18]. However, the most well-accepted collision factor is given in Eq. (2) due to its simplicity and efficiency, which is called BGK collision factor [14,15].

$$\Omega_i = \frac{1}{\tau} (f_i(x, t) - f_i^{eq}(x, t)) \quad (2)$$

f_i^{eq} is the equilibrium distribution function and τ is the relaxation factor.

$$\tau = \frac{1}{2} + 3 \frac{u \cdot N}{Re} \quad (3)$$

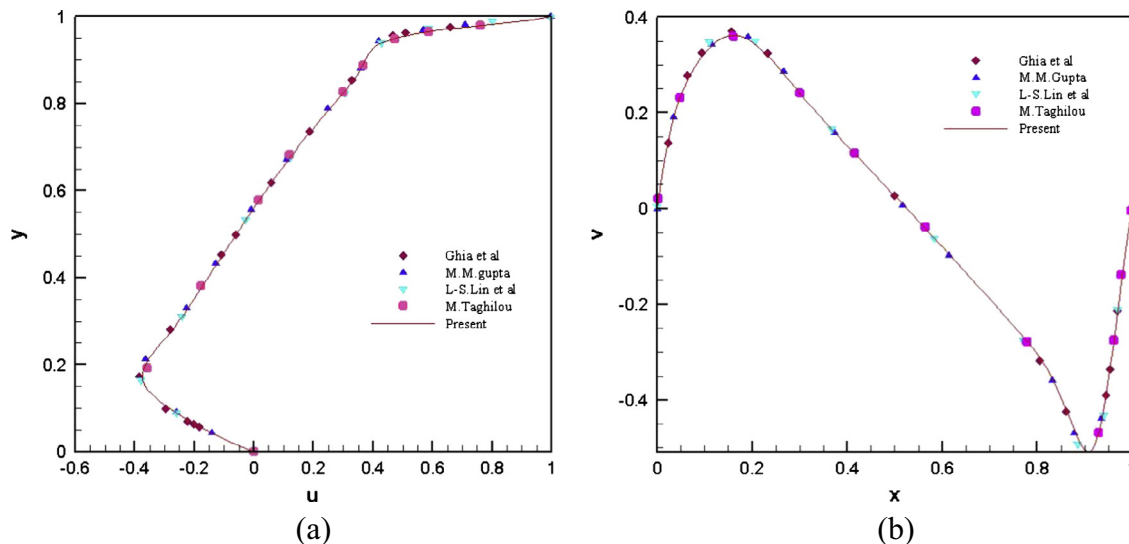
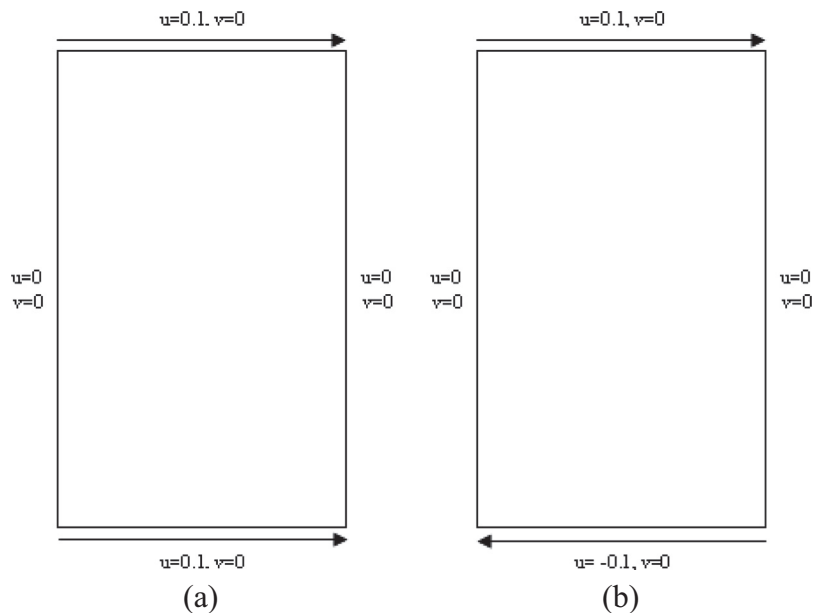


Figure 4 Comparison of predicted (a) horizontal and (b) vertical velocity with references at Reynolds number 1000 with aspect ratio $K = 1$.

Table 2 Comparisons of the locations of the vortices at various Reynolds number with other researchers solutions with aspect ratio $K = 1$.

Reynolds number		Primary vortex		Right secondary vortex		Left secondary vortex	
		x	y	x	y	x	y
Re = 100	Ghia et al. [20]	0.6172	0.7344	0.9453	0.0625	0.0313	0.0391
	Vanka [26]	0.6188	0.7375	0.9375	0.0563	0.0375	0.0313
	Schreiber, Keller [22]	0.6167	0.7417	0.9417	0.0500	0.0333	0.0250
	Hou et al. [9]	0.6196	0.7373	0.9451	0.0627	0.0392	0.0353
	Gupta [21]	0.6125	0.7375	0.9375	0.0625	0.0375	0.0375
	Pandit [24]	0.6184	0.7273	0.9425	0.0575	0.0316	0.0439
	Lin et al. [12]	0.6140	0.7323	0.9448	0.0591	0.0346	0.0342
	Present Study	0.6140	0.7324	0.9461	0.0572	0.0347	0.0347
Re = 400	Ghia et al. [20]	0.5547	0.6055	0.8906	0.1205	0.0508	0.0469
	Vanka [26]	0.5563	0.6000	0.8875	0.1188	0.0500	0.0500
	Schreiber, Keller [22]	0.5571	0.6071	0.8857	0.1143	0.0500	0.0429
	Hou et al. [9]	0.5608	0.6078	0.8902	0.1255	0.0549	0.0510
	Gupta [21]	0.5500	0.6125	0.8875	0.1250	0.0500	0.0500
	Pandit [24]	0.5532	0.6055	0.8908	0.1384	0.0528	0.0439
	Lin et al. [12]	0.5543	0.6024	0.8875	0.1206	0.0510	0.0468
	Mishra, Sanyasiraju [25]	0.563	0.604	0.896	0.120	0.063	0.042
Present Study	0.5567	0.6029	0.8891	0.1201	0.0496	0.0462	
Re = 1000	Ghia et al. [20]	0.5313	0.5625	0.8594	0.1094	0.0859	0.0781
	Vanka [26]	0.5438	0.5625	0.8625	0.1063	0.0750	0.0813
	Schreiber, Keller [22]	0.5286	0.5643	0.8643	0.1071	0.0857	0.0714
	Hou et al. [9]	0.5333	0.5647	0.8667	0.1137	0.0902	0.0784
	Botella, Peyret [27]	0.5308	0.5652	0.8711	0.1094	0.0859	0.0820
	Bruneau, Jouron [23]	0.5313	0.5586	0.8640	0.1118	0.0833	0.0781
	Gupta [21]	0.5250	0.5625	0.8625	0.1125	0.0875	0.0750
	Pandit [24]	0.5266	0.5532	0.8577	0.1092	0.0840	0.0840
	Lin et al. [12]	0.5309	0.5645	0.8652	0.1117	0.0833	0.0776
	Mishra, Sanyasiraju [25]	0.531	0.563	0.859	0.109	0.086	0.078
	Present Study	0.5315	0.5632	0.8664	0.1119	0.0826	0.0767

**Figure 5** Geometry boundary conditions for (a) same direction (b) opposite direction wall motions.

N indicates the number of lattices in direction of characteristic length. From the local Maxwell–Boltzmann model, the equilibrium distribution function can be obtained [11,14].

$$f_i^{eq}(x) = \omega_i \rho(x) \left[1 + 3c_i \cdot u + \frac{9}{2}(c_i \cdot u)^2 - \frac{3}{2}u^2 \right] \quad (4)$$

In Eq. (4) ω_i is the weight factor at respective lattice, ρ and u denote the macroscopic density and velocity respectively. The weight factors differ with respect to the model used. For D2Q9 model the weight factors are [14]

$$\omega_i = \begin{cases} \frac{4}{9} & i = 0 \\ \frac{1}{9} & i = (1, 2, 3, 4) \\ \frac{1}{36} & i = (5, 6, 7, 8) \end{cases} \quad (5)$$

After discretizing and applying the BGK collision factor in the Boltzmann equation [14]

$$f_i(x + c_i \Delta t, t + \Delta t) = f_i(x, t) - \frac{1}{\tau} [f_i(x, t) - f_i^{eq}(x, t)] \quad (6)$$

by applying the above equation, the distributive functions at each lattice points are updated. The above equation is usually solved in two sub-steps.

Collision step

$$\tilde{f}_i(x, t + \Delta t) = f_i(x, t) - \frac{1}{\tau} [f_i(x, t) - f_i^{eq}(x, t)] \quad (7)$$

Streaming step

$$f_i(x + c_i \Delta t, t + \Delta t) = \tilde{f}_i(x, t + \Delta t) \quad (8)$$

where \tilde{f}_i is the post collision function. The lattice velocity (c_i) for D2Q9 model [11–16] is given below

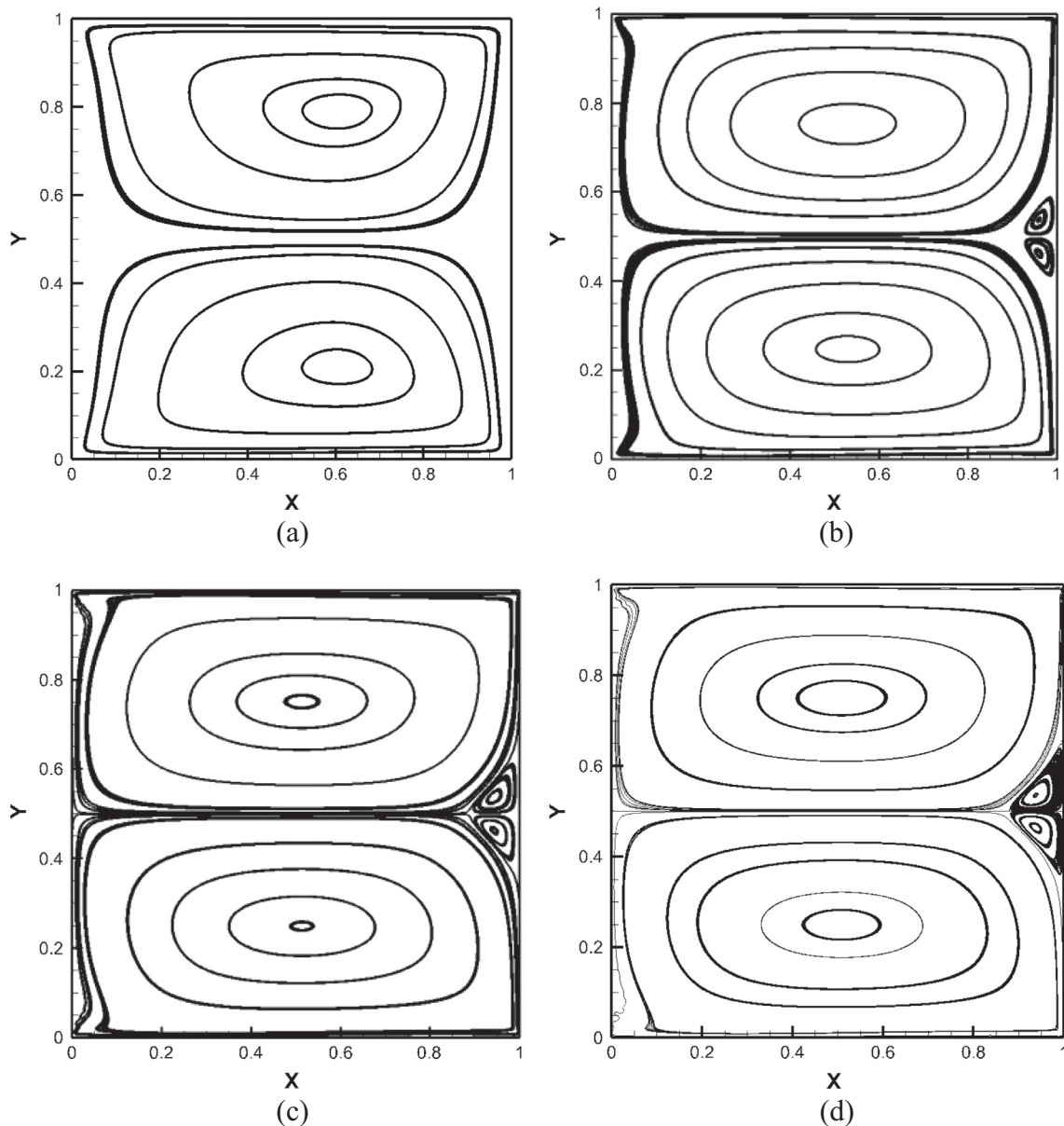


Figure 6 Streamline at steady state condition for $K = 1$ (a) $Re = 100$ (b) $Re = 1000$ (c) $Re = 2000$ (d) $Re = 5000$.

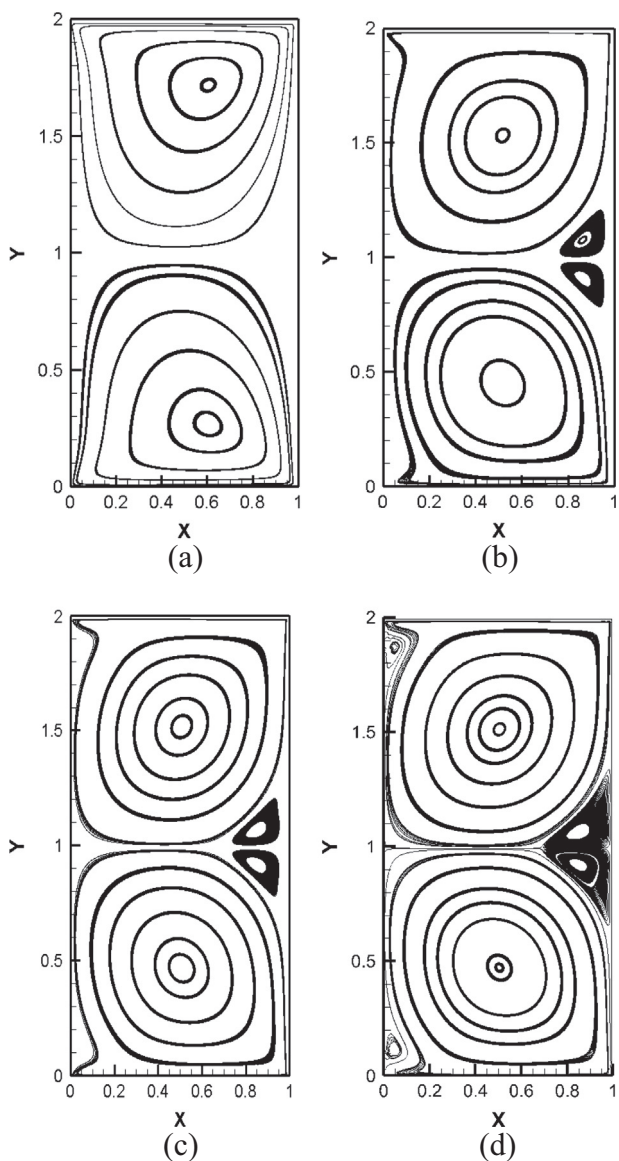


Figure 7 Streamline at steady state condition for $K = 2$ (a) $Re = 100$ (b) $Re = 1000$ (c) $Re = 2000$ (d) $Re = 5000$.

$$c_i = \begin{cases} (0,0) & i=0 \\ c[\sin(i-1)\pi/2], [\cos(i-1)\pi/2] & i=1,2,3,4 \\ c(\sqrt{2}[\cos(2i-11)\pi/4], \sqrt{2}[\sin(2i-11)\pi/4]) & i=5,6,7,8 \end{cases} \quad (9)$$

The macroscopic quantities (velocity U , pressure p , mass density ρ , momentum density ρu .) are obtained by evaluating the distribution function f . The macroscopic quantities are calculated as

$$\text{Fluid density } \rho = \sum_{i=0}^{\beta-1} f_i \quad (\beta = 9) \quad (10)$$

$$\text{Velocity } U = \frac{1}{\rho} \sum_{i=0}^{\beta-1} f_i c_i \quad (\beta = 9) \quad (11)$$

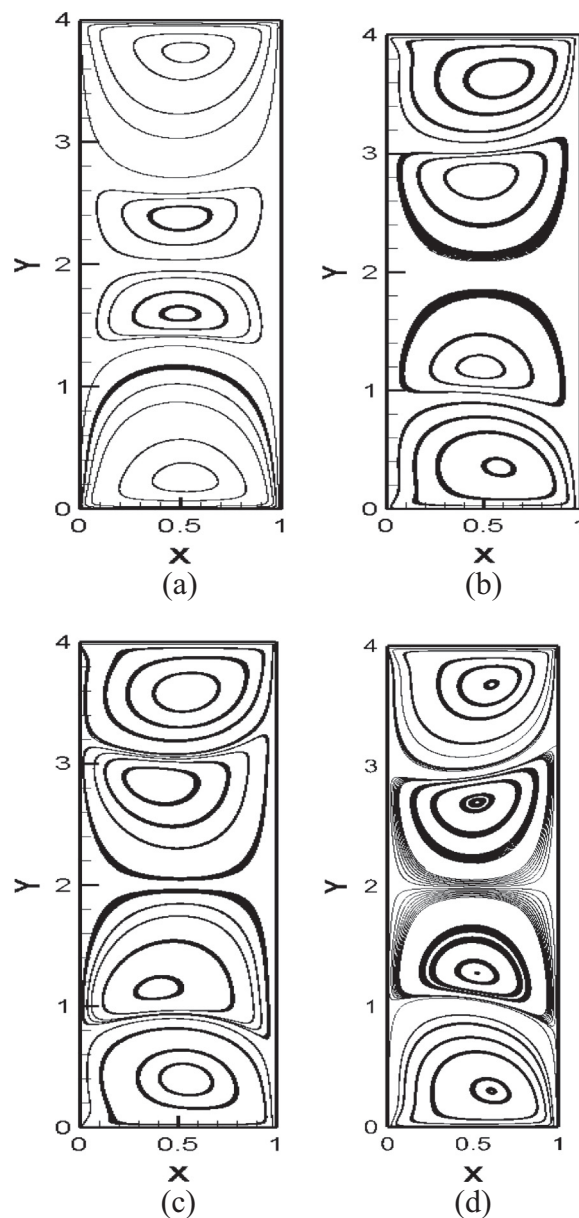


Figure 8 Streamline at steady state condition for $K = 4$ (a) $Re = 100$ (b) $Re = 1000$ (c) $Re = 2000$ (d) $Re = 5000$.

The boundary conditions play a significant role in any kind of the simulation process. In LBM, the simple bounce back and no-slip boundary condition is widely used. Fig. 5 shows the boundary conditions applied at the four walls of the cavity used in the present study.

3. Methodology

In LBM, $D\alpha Q\beta$ represents the models, where the Greek symbols α is an integer number denoting the space dimensionality and β refers to the number of discrete velocities. In this present work, a two-dimensional problem is considered. For solving fluid flow problems, D2Q9 models are most generally used [19]. It has high-velocity vectors, with the middle particle speed, being zero. Fig. 1 shows the illustration of D2Q9 model.

In this work, the Single relaxation Time BGK collision factor is used. This SRT-BGK model is considered as the simple and efficient collision factor for solving fluid flow problems by LBM. Only lower Re is selected in this present work, so SRT model is considered. A convergence criterion of $1e-10$ is fixed in the present analysis to obtain stable solutions.

4. Results and discussions

The performance of two-sided shallow lid-driven cavity is discussed for different Re ranging from 100 to 5000 and at different aspect ratio. The results are presented in terms of stream function, mid-plane u and v velocities and pressure contours. For achieving stability results and better accuracy, SRT-BGK model is used in D2Q9 (as shown in Fig. 1) lattice configuration. It is known that, greater the grid size or lattice size, greater is the accuracy of the simulation but it is not possible to use very high grid size because of its main drawback, that is the computational time and memory consumption. As the grid size increases, the time and space needed for the computation increases. In order to obtain the acceptable accuracy with less time, there is a need for finding the optimum grid size. Therefore, the present simulations are performed for lid-driven cavity at $Re = 1000$ with different lattice sizes. The schematic of the geometry and boundary conditions used for grid-independent test is shown in Fig. 2 and its results are reported in Fig. 3. The vertical mid-plane u -velocity and horizontal mid-plane v -velocity clearly describe that the deviation of results for various lattice sizes. Table 1 shows the locations of primary and secondary vortices obtained for Reynolds number 1000 and aspect ratio $K = 1$ for different grid sizes. The results obtained from these simulations show that the differences are nearly marginal, especially after the grid size of 129×129 and above as shown in Table 1. This result was also shown in the work by Lin et al. [12] and concluded that the mesh sizes have less effect on solutions accuracies especially when the grid sizes are greater than 129×129 . Hence, to save the time and space consumption, all the simulations are done by keeping 129-lattice size as a base size and for higher aspect ratio, the proportion of 129-lattice size is used.

For the validation purpose, lid-driven cavity benchmark results [12,20–22] are compared with the results obtained from the LBM code for the same square cavity and boundary conditions shown in Fig. 2. Fig. 4 demonstrates that the steady state condition, the u -velocity along vertical centerline and v -velocity along horizontal centerline at $Re = 1000$ of the present work is unmistakably in concurrence with the previous literatures. Also for more clarification of the code, the locations of primary vortex and two bottom secondary vortices are compared with the solutions of many researchers [12,20–27] for $Re = 100, 400$ and 1000 with $K = 1$ and it is listed in Table 2.

4.1. Wall movements in the same direction

Fig. 5(a) shows that the top and bottom walls move in the same direction with non-dimensional u -velocity as 0.1. The other two walls are kept stationary. For $K = 1$, the streamline flow patterns of the lid driven cavity at steady state condition are presented in Fig. 6. From the results, it is observed that each velocity vector makes it essential vortex. For Reynolds

number 100 two primary vortices that are symmetrical along the horizontal line are seen turning towards the velocity direction. However, when Re increases there is a formation of secondary vortex that pivots in the inverse course to the applied velocity near the right boundary and the flow patterns are symmetric along the horizontal mid-plane. The secondary vortex size gradually increases as the Reynolds number increases. However, there is no much variation observed in the higher Re between 2000 and 5000. As aspect ratio increases, the streamline patterns are elongated towards the centre of the shallow cavity. However, the vortex is observed close to the respective walls as shown in Fig. 7(a). For $Re = 100$ and $K = 2$, there is no formation of secondary vortices. As Re increases, the vortex is moved towards the half of vertical centre plane with respect to the lid movement and the apparent

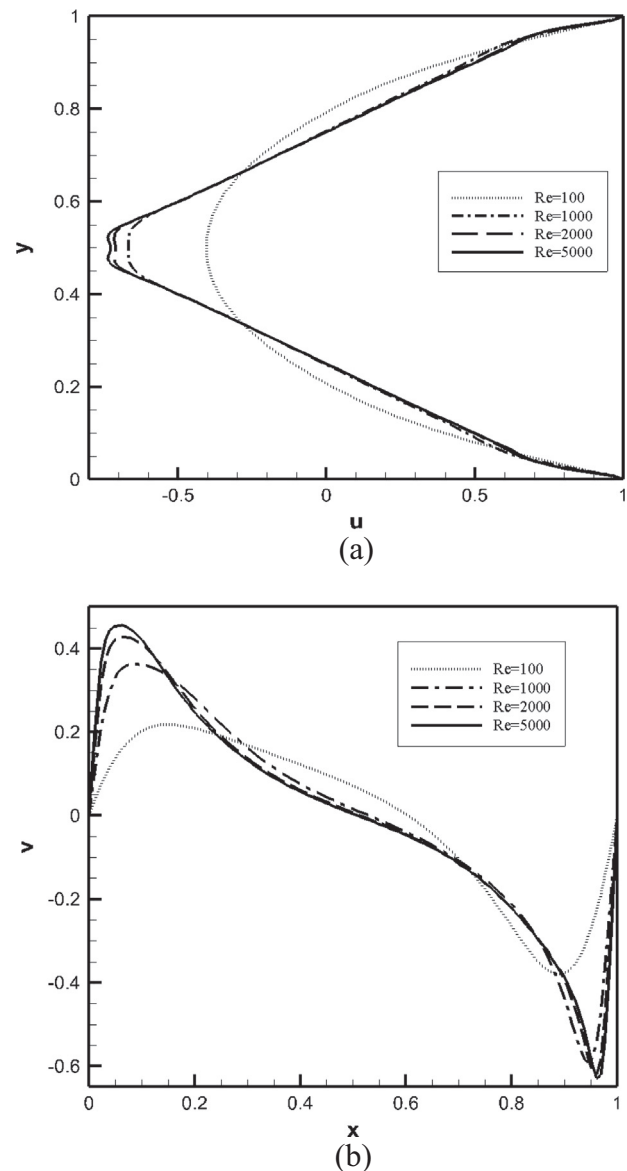


Figure 9 (a) horizontal velocity along vertical centerline and (b) vertical velocity along horizontal centerline for various Reynolds number for aspect ratio $K = 1$.

of secondary vortices are shown clearly in Fig. 7(b). The verge of ternary vortices is also observed near the top and bottom left corners. For $Re = 2000$ and 5000 , the location of each primary vortex is exactly at the mid point of the vertical plane and the formation of ternary vortices is observed at $Re = 5000$ (shown in Fig. 7d). It is observed from the present results that the four primary vortices are seen for the deep shallow cavity ($K = 4$) even at low Reynolds number ($Re = 100$) itself as shown in Fig. 8. However, the shape and size of those primary vortices increase with the increase of Reynolds number. The secondary vortex forms at the initial stage are merged with the primary vortices, thus resulting in the evolution of primary vortices. This effect is similar to the results shown in the work of Patil et al. [30].

The midplane u - and v -velocities for different Reynolds numbers and aspect ratio of 1 is shown in Fig. 9. For low Re , the vortex formation is observed near the top wall ($u = 0$) at approximately $y/H = 0.75$. As Re increases, the vortex is positioned perfectly at the mid of the vertical plane. It is also observed from Fig. 9(a) that the u -velocity for $Re = 100$ is 0.4 with opposite to the lid directions, and it is found to decrease with an increase in Re . Similarly, the variations of v -velocity at the horizontal midplane are presented in Fig. 9(b). As the left and right boundaries are kept stationary, the vertical velocity within the cavity is distributed, and it is found that the increase in Re has many collisions on the v -velocity. The pressure contours for $Re = 100$ and at different aspect ratio is shown in Fig. 10. As the lids are moving in the same direction, the adverse pressure towards the centre of the cavity is plotted. However, the pressure disorder is insignificant. As shown in Fig. 10 the pressure is maximum in the top left wall and bottom left wall. As mentioned in the streamline the pressure contours also symmetry along the horizontal line. When the aspect ratio increases the pressure developed at the centre of the cavity is also almost maximum. As it can be observed from the result even though the pressure distribution

is not varied much inside the cavity, the maximum pressure obtained only in the above mentioned locations.

4.2. Walls movements in opposite direction

The effects of the top wall moves from left to right and bottom wall moves from right to left with the same magnitude on streamline and pressure contours are discussed. Fig. 5(b) shows the schematic representation of wall movement of the top and bottom wall of the cavity and the sidewalls are kept stationary. Fig. 11 shows the streamline pattern for $K = 1$ for various Re at steady state conditions. From the results, it is observed in the initial state there is a formation of two primary vortices but after few iterations the two vortices merges together because of the opposite wall motion and form a single primary vortex. When Re increases, there is a formation of secondary vortex, which flows in the inverse direction to the applied velocity. Since the walls moves opposite direction the secondary vortex are found at the top left and bottom right instead of near the horizontal mid plane as observed in the previous case. From Fig. 11 it is also observed clearly the shape and size of the secondary vortex increases with an increase in Re . When the aspect ratio is increased ($K = 2$) for $Re = 100$, the single primary vortex started to divide into two primary vortex and forms a sand clock like pattern as shown in Fig. 12(a). It is observed at the mid vertical plane the vortex begins to divide. When Re increases and due to the elongated aspect ratio the streamlines appears to be elongated and form an eye shaped pattern at the middle of the cavity and towards the driven walls the streamlines are flattened. For still higher Re the secondary vortex gains the size by comprising the primary vortex. Fig. 13 shows the streamline patterns for $K = 4$. For $Re = 100$, two separate primary vortices are formed for each velocity and in addition to that there is a formation of sand clock like pattern at the middle of the

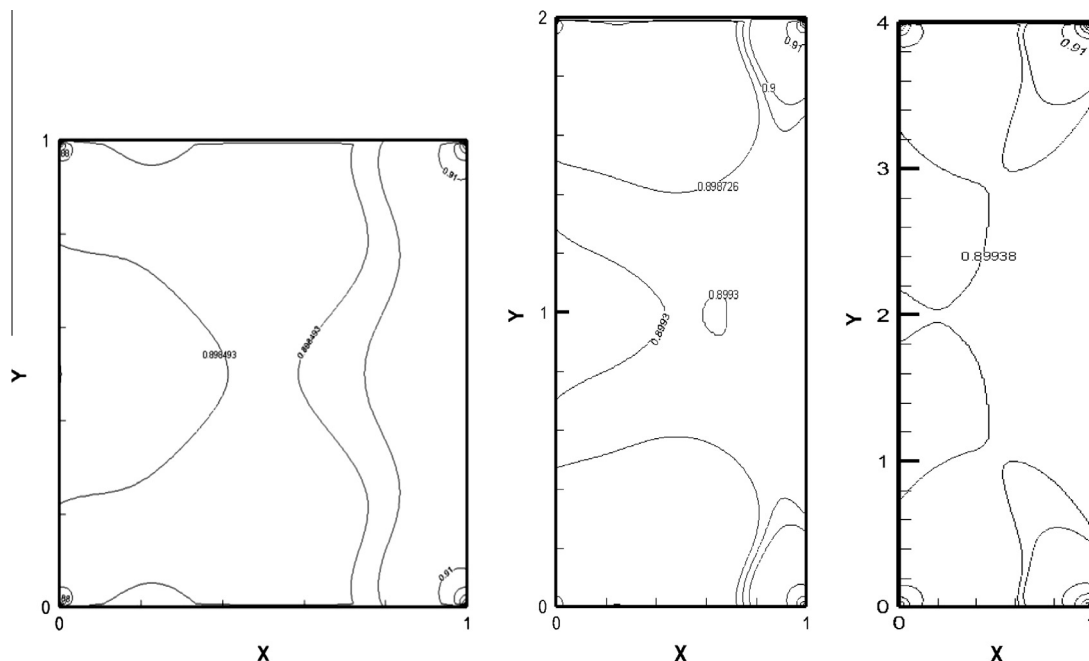


Figure 10 Pressure contour for same direction $Re = 100$ and $K = 1, 2, 4$.

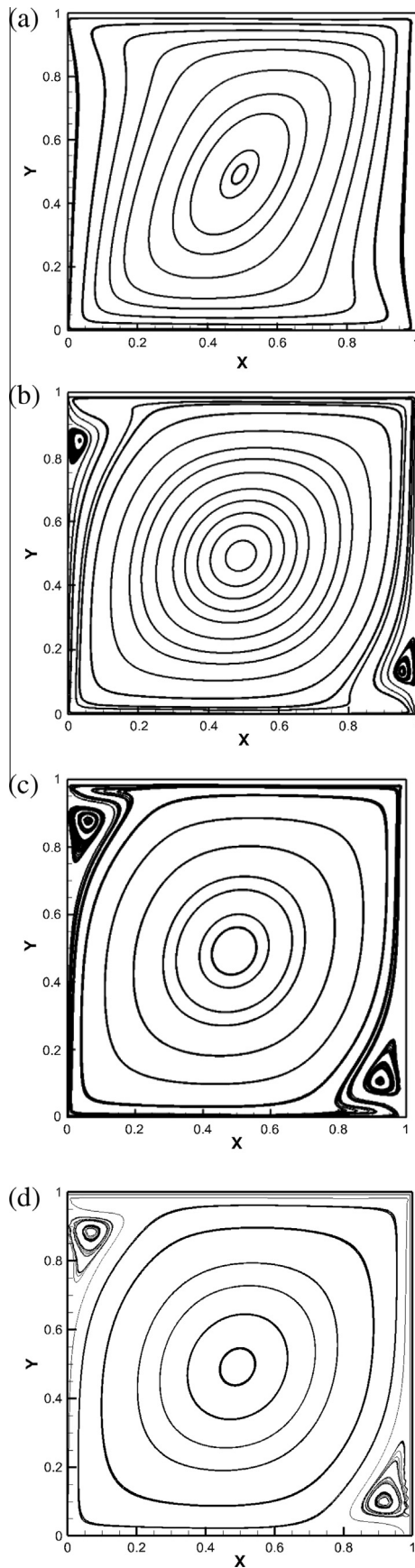


Figure 11 Streamline at steady state condition for $K = 1$ (a) $Re = 100$ (b) $Re = 1000$ (c) $Re = 2000$ (d) $Re = 5000$.

cavity as discussed before. Fig. 13(b) and (c) shows that when Re is increased for this aspect ratio, the secondary vortices is not observed as seen in other aspect ratios instead of that many primary vortices emerges, because of the vortex evolution as explained in previous case. The shape of these vortices changes with Re . When Re is still increased to 5000, very small corner vortices are observed.

Fig. 14 shows the midplane u and v -velocities for different Reynolds numbers and aspect ratio of 1. The maximum velocity in the top wall is represented as 1 in the graph and the bottom wall as -1 since this wall moves in opposite direction. For lower Re (100) u velocity forms the S-shaped profile. When Re increases, there is a linear change in the velocity profile in the middle of the cavity and sudden increase as it reaches near the wall. The vertical velocity increases from zero and starts decreases in the middle of the cavity and once again it increases finally reaches zero at the wall. For higher Re , the increase of velocity is sharper and gradually decreases. Fig. 15 represents the pressure generated in the cavity (when Re 100) due to the

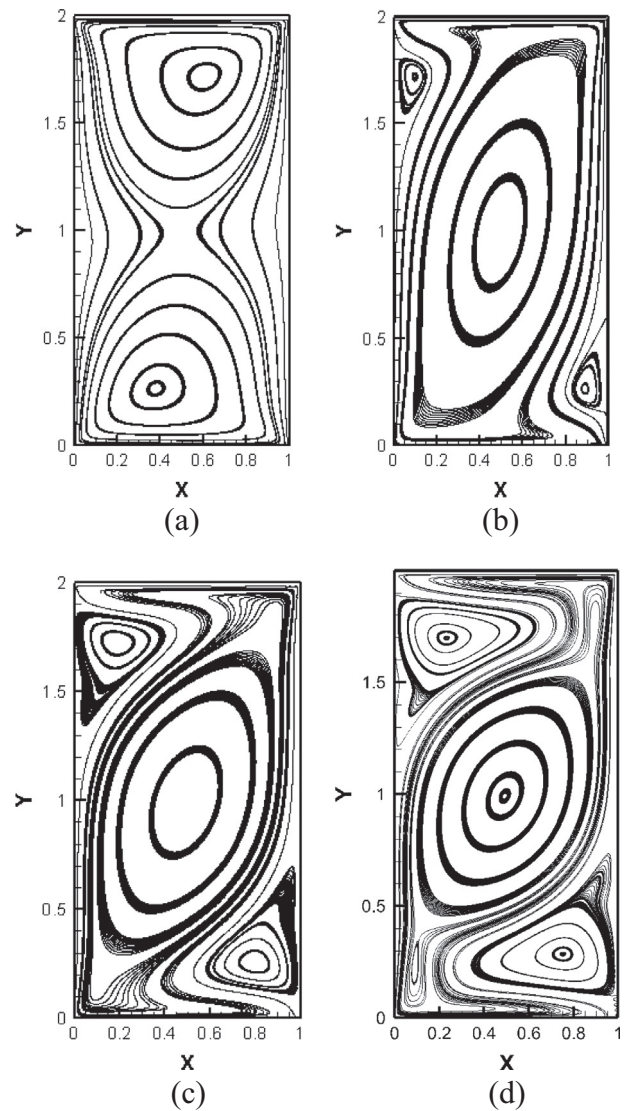


Figure 12 Streamline at steady state condition for $K = 2$ (a) $Re = 100$ (b) $Re = 1000$ (c) $Re = 2000$ (d) $Re = 5000$.

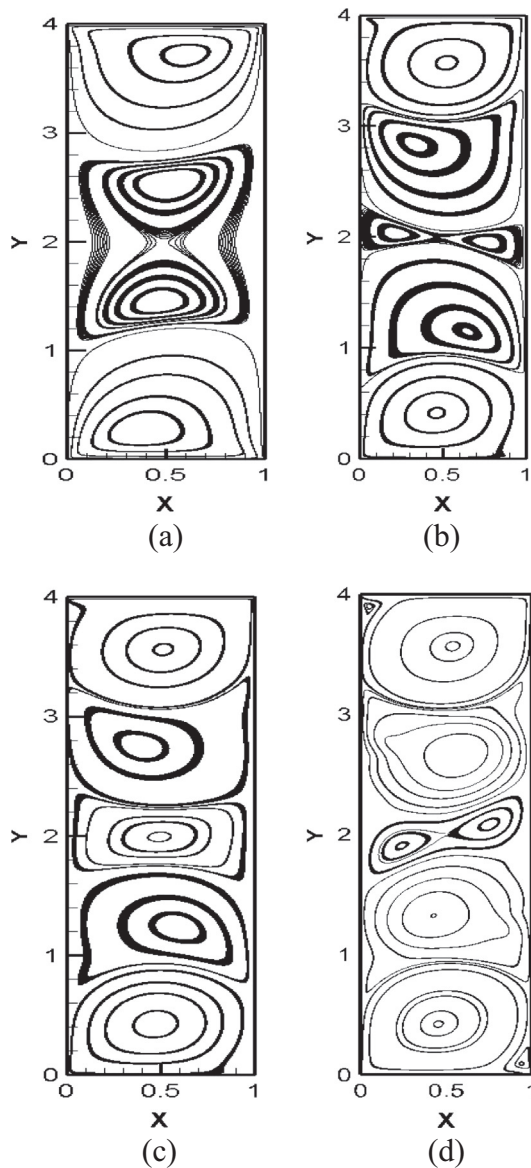


Figure 13 Streamline at steady state condition for $K = 4$ (a) $Re = 100$ (b) $Re = 1000$ (c) $Re = 2000$ (d) $Re = 5000$.

walls moves in opposite direction are shown and clearly indicates the distribution of pressure for different aspect ratios (1, 2, and 4). The maximum pressure is observed in the top right and bottom left wall of the cavity which corresponds with the wall movement. As mentioned in the previous case, when the aspect ratio increases the pressure is developed along the horizontal centre line of the cavity is almost equal to the maximum pressure. In rest of the locations the pressure distributions are found to be in equal. Further for $K = 4$ the centre area where the maximum pressure developed is increased. Only the areas near the top left and bottom right corner of the cavity the pressure intensity is considerably less when compared with the other areas.

5. Conclusions

In this present work the flow attributes in a cavity, where the top and bottom walls moves in same and opposite direction

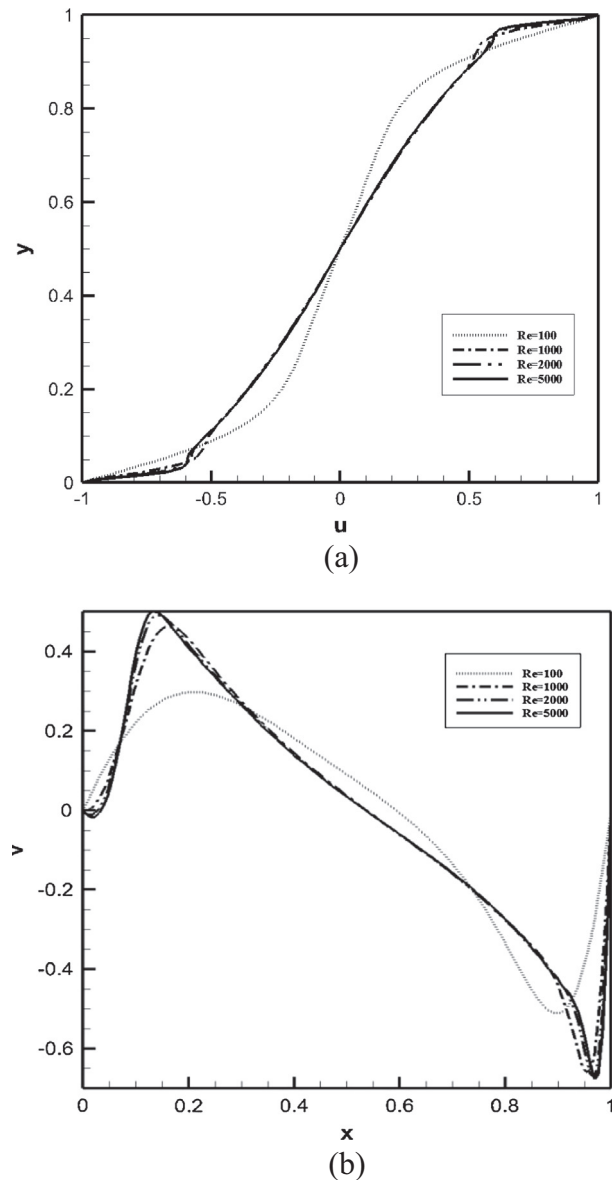


Figure 14 (a) horizontal velocity along vertical centerline and (b) vertical velocity along horizontal centerline for various Reynolds number for aspect ratio $K = 1$.

is studied in detail by using LBM concepts. The 2d incompressible flow was defined by D2Q9 model with SRT collision factor. For moving wall Zou and He [19] boundary condition is applied and for stationary walls bounce back boundary condition is applied. The code is validated with benchmark problem and good agreement is obtained. For the present work the simulation is done for various Reynolds number (100, 1000, 2000 and 5000) and aspect ratios (1, 2, and 4) to understand the effects of Re and K in the flow attributes. Very interesting results are obtained from the simulation. The different streamline patterns, velocity profile and pressure contours are explained detail in the above section. Different shapes and sizes of streamline patterns are obtained for various Re and K . The results shows for $K = 4$, no secondary vortex formed even for higher Re for the walls move in same direction but for the walls moving in opposite direction for $Re = 5000$ small

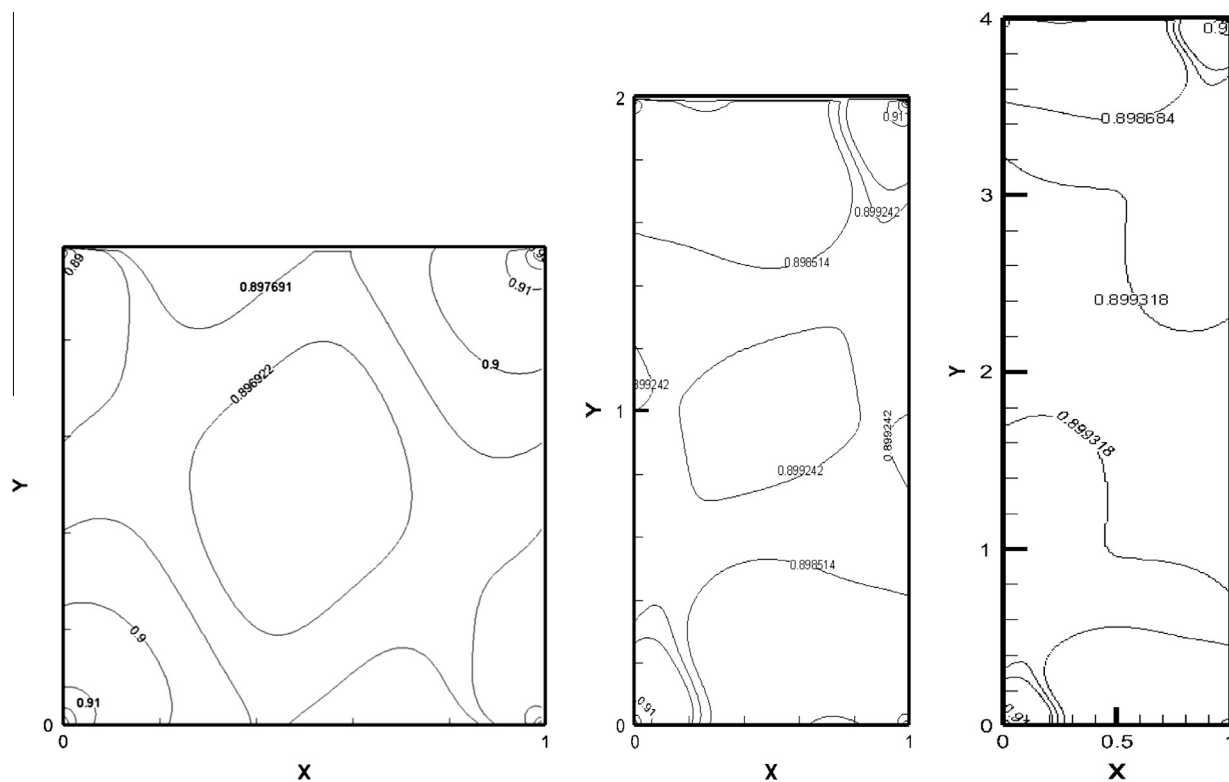


Figure 15 Pressure contour for opposite direction $Re = 100$ $K = 1, 2, 4$.

secondary vortex are found. The graphs of u and v velocity describe the velocity profile formed in the cavity. The distribution of pressure because of the wall motions for different Re is also analysed.

References

- [1] Y.Y. Yan, Y.Q. Zu, B. Dong, LBM, a useful tool for mesoscale modelling of single-phase and multiphase flow, *Appl. Therm. Eng.* 31 (2011) 649–655.
- [2] H. Nemati, M. Farhadi, K. Sedighi, E. Fattahi, A.A.R. Darzi, Lattice Boltzmann simulation of nanofluid in lid-driven cavity, *Int. Commun. Heat Mass Transfer* 37 (2010) 1528–1534.
- [3] Q. Dai, L. Yang, LBM numerical study on oscillating flow and heat transfer in porous media, *Appl. Therm. Eng.* 54 (2013) 16–25.
- [4] T. Sun, W. Li, S. Yang, Numerical simulation of bubble growth and departure during flow boiling period by lattice Boltzmann method, *Int. J. Heat Fluid Flow* 44 (2013) 124–139.
- [5] M. Sheikholeslami, M.G. Bandy, D.D. Ganji, S. Soleimani, S.M. Seyyedi, Natural convection of nanofluids in an enclosure between a circular and a sinusoidal cylinder in the presence of magnetic field, *Int. Commun. Heat Mass Transfer* 39 (2011) 649–655.
- [6] M. Jourabian, M. Farhadi, A.A.R. Darzi, Simulation of natural convection melting in an inclined cavity using lattice Boltzmann method, *Scientia Iranica* 19 (2012) 1066–1073.
- [7] S. Chen, G. Doolen, Lattice Boltzmann method for fluid flows, *Annu. Rev. Fluid Mech.* 30 (1998) 329–364.
- [8] C.K. Aidun, N. Triantafillopoulos, J. Benson, Global stability of a lid-driven cavity through flow: Flow visualization studies, *Phys. Fluids A* (1991).
- [9] S. Hou, Q. Zou, S. Chen, G. Doolen, A. Cogley, Simulation of cavity flows by the lattice Boltzmann method, *J. Comput. Phys.* 118 (1995) 329–347.
- [10] M.A. Mussa, S. Abdullah, C.S.N. Azwadi, N. Muhamad, K. Sopian, Numerical Simulation of Lid-Driven Cavity Flow Using the Lattice Boltzmann Method, In: *Proceedings of the 13th WSEAS International Conference on Applied Mathematics*, 2008, pp. 236–240.
- [11] M. Taghilou, Simulation of lid driven cavity flow at different aspect ratios using single relaxation time lattice boltzmann method, *Int. J. Eng.* 26 (2012) 1471–1478.
- [12] L.S. Lin, Y.C. Chen, C.A. Lin, Multi relaxation time lattice Boltzmann simulations of deep lid driven cavity flows at different aspect ratios, *Comput. Fluids* 45 (2011) 233–240.
- [13] F. Yang, X. Shi, X. Guo, Q. Sai, MRT Lattice Boltzmann Schemes for high Reynolds number flow in two-dimensional lid-driven semi-circular cavity, *Energy Procedia* 16 (2012) 639–644.
- [14] A.A. Mohamad, *Lattice Boltzmann Method Fundamentals and Engineering Applications with Computer Codes*, Springer-Verlag London Limited, 2011.
- [15] P.L. Bhatnagar, E.P. Gross, M. Krook, A model for collision processes in gases. i. small amplitude processes in charged and neutral one-component systems, *Physical Review* 94 (1954) 511–525.
- [16] I. Ginzburg, Equilibrium-type and link-type lattice Boltzmann models for generic advection and anisotropic-dispersion equation, *Advanced Water Resources* 28 (2005) 1171–1195.
- [17] A. Mwezhab, M.A. Moussaoui, M. Jami, H. Nahi, M. Bouzidi, Double MRT thermal lattice Boltzmann method for simulation convective flows, *Physics Letter A* (2010) 3499–3507.
- [18] L. Wang, Z. Guo, C. Zheng, Multi relaxation time lattice Boltzmann model for axisymmetric flows, *Comput. Fluids* 39 (2010) 1542–1548.
- [19] Q. Zou, X. He, On pressure and velocity flow boundary conditions and bounce back for the lattice Boltzmann BGK model, *Phys. Fluids* 9 (1997) 1591–1598.
- [20] U. Ghia, K.N. Ghia, C.T. Shin, High Re solutions for incompressible flow using the Navier-Stokes equations and a multigrid method, *J. Comput. Phys.* 48 (1982) 387–411.

- [21] M.M. Gupta, J.C. Kalita, A new paradigm for solving Navier-Stokes equations: streamfunction-velocity formulation, *J. Comput. Phys.* 207 (2008) 52–68.
- [22] R. Schreiber, H.B. Keller, Driven cavity flows by efficient numerical techniques, *J. Comput. Phys.* 49 (1983) 310–333.
- [23] C.-H. Bruneau, C. Jouron, An efficient scheme for solving steady incompressible Navier-Stokes equations, *J. Comput. Phys.* 89 (1990) 389–413.
- [24] S.K. Pandit, On the use of compact stream function-velocity formulation of steady Navier-Stokes equations on geometries beyond rectangular, *Journal of Science and Computers* 36 (2008) 219–242.
- [25] N. Mishra, Y.V.S.S. Sanyasiraju, Exponential compact higher order scheme for steady incompressible navier-stokes equations, *Engineering Applications of Computational Fluid Mechanics* 4 (2012) 554–568.
- [26] S.P. Vanka, Block-implicit multigrid solution of Navier-Stokes equations in primitive variables, *J. Comput. Phys.* 158 (1986) 138–158.
- [27] O. Botella, R. Peyret, Benchmark spectral results on the lid-driven cavity flow, *Comput. Fluid.* 27 (1998) 421–433.
- [28] Mohamed A. Teamah, Wael M. El-Maghlany, Numerical simulation of double-diffusive mixed convective flow in rectangular enclosure with insulated moving, *Int. J. Therm. Sci.* 49 (2010) 1625–1638.
- [29] Fakher Oueslati, Brahim Ben-Beya, Taieb Lili, Double-diffusive natural convection and entropy generation in an enclosure of aspect ratio 4 with partial vertical heating and salting sources, *Alexandria Eng. J.* 52 (2013) 605–625.
- [30] D.V. Patil, K.N. Lakhmisha, B. Rogg, Lattice Boltzmann simulation of lid-driven flow in deep cavities, *Comput. Fluid.* 35 (2006) 1116–1125.
- [31] M. Teamah, M. Sorour, W.M. El-Maghlany, Amr Afifi, Numerical simulation of double diffusive laminar mixed convection in shallow inclined cavities with moving lid, *Alexandria Eng. J.* 52 (2013) 227–239.
- [32] Mohamed A. Teamah, Wael M. El-Maghlany, Mohamed M. Khairat Dawood, Numerical simulation of mixed convection in two sided lid-driven differentially heat rectangular enclosure, *Alexandria Eng. J.* 49 (2010) 1–12.